Estimation of Torque Variation from Pedal Motion in Cycling

Quintana-Duque, J.-C., Dahmen, T., Saupe, D.

Department of Computer and Information Science, University of Konstanz, Germany

Abstract

In cycling, the pedalling technique is determined mostly by variations in the torque applied to the pedals during crank rotation. We developed and validated a method to compute these variations from the pedalling motion using an ergometer. The torque at the pedal is the sum of the torques needed to overcome all resistive forces and the torque required for any changes of angular momentum of the ergometer flywheel. This last torque is proportional to the angular acceleration of the crank. For an ergometer with almost constant brake torque, we may assume that variations in the pedal force can be extracted from the pedal motion alone. The key problem is to reliably estimate the angular pedal acceleration from noisy 3D motion capture (MoCap) or 2D video data. We projected the positional data onto a least squares fitting circle, then filtered the resulting angular time sequence by local polynomial regression. Finally, we solved the torque equilibrium equation for the pedal torque. For validation of the method, we used direct pedal torque measurement. In our experiments, pedal brake forces ranged between 100 and 250 N, and cadences of 60, 80, and 100 rpm were used. The pedal torque results from MoCap were better than from video. The results from video were close to MoCap results when a correction of the marker position was applied.

KEYWORDS: CRANK ACCELERATION, PEDALLING MOTION, NET TORQUE VARIATION, FORCE VARIATION

Introduction

Cycling is the result of the interaction between the cyclist, the bicycle, and the environmental constraints. The right selection of the variables involved in adjusting a bicycle (e.g., handle bar position, seat height, crank length, etc.), the correct body position on the bicycle, and a good pedalling technique are necessary to prevent cycling injuries and to optimize the force distribution during the pedal stroke.

Applying correctly oriented forces to the pedal (i.e., pedalling technique) is a major component of skilled performance on the bicycle. Although there is no agreement on the characteristics of the optimal pedalling technique, any desired pedalling technique can be learned and trained by indoor ergometer cycling. A training session in the lab is based on the analysis and feedback of the distribution of the applied pedal forces during each revolution of the crank. In many cases, the torque variation is enough for the training of pedalling techniques and the correction of force asymmetry between the legs. See some examples in Böhm, Siebert, and Walsh (2008) and Faria (2009).

The determination of pedal forces is fundamental to analyse cycling performance from a biomechanical point of view. Sensors implemented in the pedal have been validated in the literature for measuring force in one dimension up to three dimensions based on strain gauges or piezoelectric elements. For a list of sensors see Mornieux, Zameziati, Mutter, Bonnefoy, and Belli (2006) and Stapelfeldt, Mornieux, Oberheim, Belli, and Gollhofer (2007). A direct measure of the torque (resp., tangential force applied to the pedal that rotates the crank) requires expensive sensors, but indirect ways of calculating the torque variations are possible and presented in this contribution.

The study of pedal forces in cycling is of interest for several applications. For example, some related topics are: pedalling biomechanics (Christensen et al., 2000; Hug, Turpin, Guével, & Dorel, 2010; Kautz & Hull, 1993), limb coordination (Bini, Diefenthaeler, & Mota, 2010; Jirsa, Fink, Foo, & Kelso, 2000), human motion modeling (Franz Höchtl, Harald Böhm, & Veit Senner, 2010; Hull, Kautz, & Beard, 1991), detection and correction of asymmetry (Carpes, Rossato, Faria, & Bolli Mota, 2007; Sanderson, 1990; Smak, Neptune, & Hull, 1999), evaluation of body performance given a pedalling technique (Cannon, Kolkhorst, & Cipriani, 2007; Ettema & Loraas, 2009), cadence and workload effects on pedalling technique (Black, 1994; Rossato, Bini, Carpes, Diefenthaeler, & Moro, 2008; Stapelfeldt, Mornieux, & Gollhofer, 2006) and the influence of pedalling technique on muscular efficiency (Theurel, Crepin, Foissac, & Temprado, 2011).

In order to calculate the angular acceleration from the pedalling motion, the angular position of a point representing the angular position of the crank is differentiated twice. This is not a trivial task, because the differentiation process is noise amplifying by its very nature, (Ovaska & Valiviita, 1998). For this reason, a bandwidth differentiator with special characteristics is required for this calculation. We tested the Savitsky-Golay filter (Savitzky & Golay, 1964) from which we obtained the filtered components required for the calculation of the second derivative of the angular position of the crank. In addition, we observed the differences in our results when a correction of the marker position was applied for MoCap and video data. The physical relation between the angular acceleration of the crank and the net torque applied to the pedals is derived, allowing us to compute the net torque from our motion data. The comparison of these results with directly measured crank torque (using an SRM Torque Box[1]) provides the validation of our method.

Methods

The variation in the angular acceleration is proportional to the variation in the applied torque when the pedal brake force is constant, which can be achieved using ergometers. We propose to derive the variation in the net torque from measurements of pedal motion that can be made in the laboratory using motion-capturing or plain commercial cameras. The reconstruction of the position and the orientation of the pedal was done in two ways: 1) recording video of two LEDs, and 2) by motion capture using two active infrared markers. See the experimental setup in Figure 1.

[1] http://www.srm.de/products/torque-analysis-system/

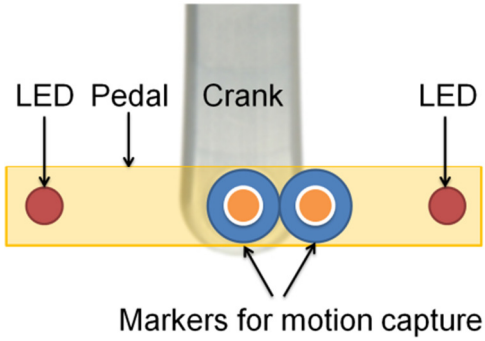

Figure 1 Pedal motion was recorded using video (through two LEDs) and motion capture (through two active infrared markers) in order to reconstruct the position and the orientation of the pedal. For motion capture one marker was placed on the pivot point of the pedal rotation and the other marker was placed to the right side of the first marker. For video the LEDs were placed on both sides of the pedal such that the midpoint between LEDs was aligned with the pivot point.

Calculation of the second derivative from positional data

We assumed that the angular position of the pivot point of rotation of the pedal and the crank angle θ with respect to the center of rotation of the crank are the same. If $(x(t), y(t))$ denote the marker coordinates of a point representing the angular position of the crank, with the origin of the coordinate system placed at the center of the crank rotation, then crank angle is given by $\theta(t) = \tan^{-1}(y(t)/x(t))$. The second derivative of θ (i.e., angular acceleration) is calculated using the chain rule for derivatives

$$\ddot{\theta} = \frac{d^2}{dt^2}\tan^{-1}\frac{y}{x} = \frac{(\ddot{y}x - y\,\ddot{x})(x^2 + y^2)}{(x^2 + y^2)^2} - \frac{(\dot{y}x - \dot{x}y)(2x\dot{x} + 2y\dot{y})}{(x^2 + y^2)^2}. \qquad (1)$$

In our application, the Savitsky-Golay filter is applied separately to the x- and y-coordinates of the pedal motion to obtain smoothed data and its first and second derivatives. This filter is briefly reviewed in the next section.

Savitzky-Golay smoothing filter

The recordings of the pedal position with motion capture data (MoCap) and video data contain noise. This noise, viewed in the frequency domain, is amplified in the calculation of the second derivative by a factor of $4\pi^2 f^2$ with f being the frequency. In order to increase the signal-to-noise ratio without greatly distorting the signal, we used the Savitzky-Golay filter (Savitzky & Golay, 1964), also known as polynomial smoothing (Hamming, 1989) or as least-squares smoothing filters (Schafer, 2011).

The Savitzky-Golay filter is a method for data smoothing based on an approximation by a local least-squares polynomial. This filter reduces the noise while maintaining the shape and height of the waveform peaks (e.g., their relative widths and heights), (Press, Teukolsky, Vetterling, & Flannery, 2007). This filter is a generalization of the FIR averaging filter. It can preserve the high frequency content of the desired signal, at the expense of not removing as much noise as the averager, (Orfanidis, 2010).

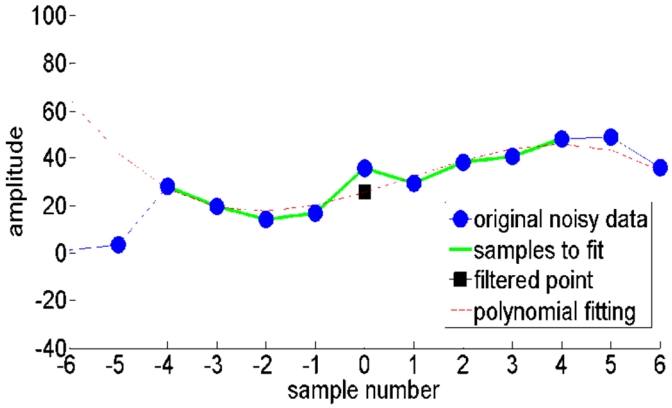

Figure 2 Example of polynomial smoothing. The smoothed output value (black square) is obtained by evaluating a polynomial of order N = 3 (red line) fitted on a group of 2M + 1 samples (on the green line), here with half-length M = 4, at n = 0.

The basic idea of this filter is to fit a polynomial to a set of consecutive input samples and then evaluate the resulting polynomial at the central point. Figure 2 shows an example of polynomial smoothing for the central point $n = 0$. The input $x[k]$, with $k \in \mathbb{Z}$, is a sequence of discrete points (solid blue dots). A window (i.e., points on the green line) with a window size of $2M + 1$ data points, with $M \geq 1$, is used to calculate a least-squares polynomial fit (here $2M + 1 = 9$). A polynomial $p[k]$ of degree $N = 3$ (red dashed line) is fitted to the data $x[k]$, with $k = n - M, \ldots, n + M$ and the smoothed output value (black square) is obtained by evaluating $p[k]$ for $k = n$. We obtain the coefficients a_i of the polynomial p of order N,

$$p[k] = \sum_{i=0}^{N} a_i k^i \,, \tag{2}$$

that minimizes the mean-squared approximation error ϵ_n for the group of input samples centered on n,

$$\epsilon_n = \sum_{m=-M}^{M} (p[n+m] - x[n+m])^2. \tag{3}$$

It can be shown that this is equivalent to discrete convolution with a fixed impulse response, (Schafer, 2011). Savitzky and Golay (1964) published tables of filter coefficients for combined smoothing and differentiation. These tables are given for two parameters: the half-length of the fitting window, M, and the order of the fitted polynomial, N. The dependence of the cutoff frequency f_c on N and M is given by

$$f_c = \frac{N+1}{3.2M - 4.6} \tag{4}$$

for $M \geq 25$ and $N \leq M$. Sometimes the same cutoff frequency can be achieved using different combinations of N and M.

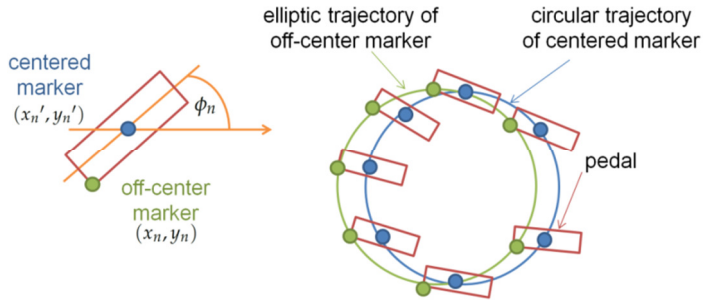

Figure 3 An off-center marker on the pedal gives a trajectory that is not a circle when the pedal orientation is not constant.

Correction of the marker position

The crank rotation during pedaling motion ideally takes place in a two dimensional plane. We expect that any marker on the crank, except the pivot of crank rotation, describes a perfect (sampled) circular trajectory. The angular position of the crank can be obtained from the trajectory of a point representing the angular position of the crank. In the same way, the angular position can be calculated from the trajectory described by a marker on the pedal, provided that the marker is on the pivot of pedal rotation. Otherwise the marker trajectory turns into an approximate ellipse due to simultaneous rotations of pedal and crank. See Figure 3.

However, although the marker position is on the pivot of pedal rotation, the crank and pedal rotations in the real world describe an elliptical trajectory because the bearings at the pedals and in the bottom bracket may have small play and the crank sets are slightly elastic.

The eccentricity of an ellipse fitted to the marker trajectory characterizes the amount by which the marker trajectory deviates from a circle. The eccentricity e is defined as $e = \sqrt{1 - b^2/a^2}$ with a and b denoting the length of the major and minor axes, respectively.

The correction $(\Delta x, \Delta y)$ of the 2D position of a marker on the pedal can be calculated if the pedal orientation ϕ_n with respect to the horizontal axis is known. The correction of the marker position is given by

$$\begin{pmatrix} x_n' \\ y_n' \end{pmatrix} = \begin{pmatrix} x_n \\ y_n \end{pmatrix} + \begin{pmatrix} \cos\phi_n & -\sin\phi_n \\ \sin\phi_n & \cos\phi_n \end{pmatrix} \begin{pmatrix} \Delta x \\ \Delta y \end{pmatrix}, \quad (5)$$

where x_n and y_n are the old coordinates, x_n' and y_n' are the new coordinates after correction. The correction vector $(\Delta x, \Delta y)$ is defined such that: either 1) a prescribed target eccentricity of an ellipse fitted to the corrected positional data is achieved (in following called „prescribed eccentricity“) or 2) the RMS distance between the fitted ellipse and the corrected data is minimal among all possible corrections and their respective fitted ellipses (in following called „minimum error eccentricity M.E.“).

Related concepts: force and torque

The total force $\mathbf{F}_{\text{total}}$ applied to the pedal is the sum of all vector forces, see Figure 4, produced by the contractions and extensions of the leg and hip muscles which can be decomposed into tangential and radial forces, $\mathbf{F}_{\text{tan}}$ and $\mathbf{F}_{\text{rad}}$, respectively (Equation 6). The force $\mathbf{F}_{\text{tan}}$ is tangential to the crank rotation and the radial force $\mathbf{F}_{\text{rad}}$ is parallel to the crank. Only $\mathbf{F}_{\text{tan}}$ contributes to the crank rotation,

$$\mathbf{F}_{\text{total}} = \mathbf{F}_{\text{tan}} + \mathbf{F}_{\text{rad}}. \quad (6)$$

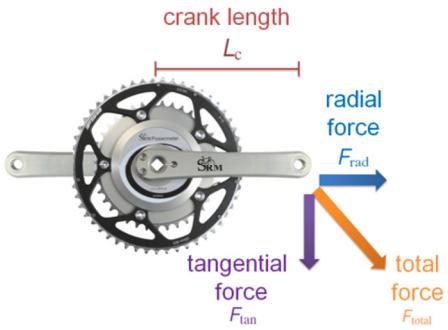

Figure 4 The total force applied to the pedal, $\mathbf{F}_{\text{total}}$, is the sum of two perpendicular forces: the tangential $\mathbf{F}_{\text{tan}}$ and the radial force $\mathbf{F}_{\text{rad}}$.

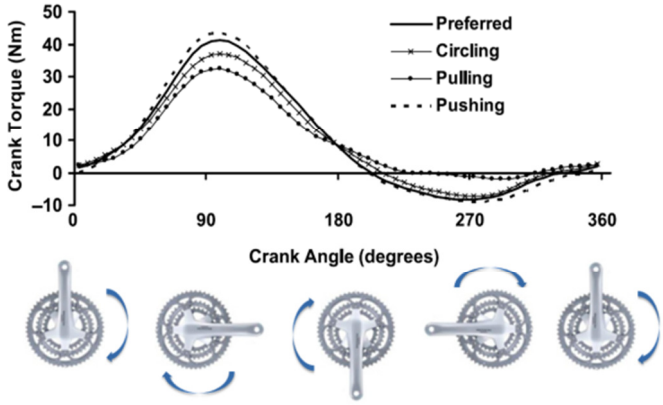

Figure 5 Right leg torque profiles using different pedalling styles at 90 rpm and 200 W. Figure adapted from Korff, Romer, Mayhew, and Martin (2007). Four pedalling styles are shown: individually preferred pedalling technique (preferred), pedalling emphasizing the transition phases through top dead center at 0° and bottom dead center of the crank cycle at 180° (circling), emphasizing an active pull during the upstroke of the crank cycle (pulling), and emphasizing the pushing action during the downstroke of the crank cycle (pushing).

The torque describes the effect of a force on the rotational motion of the pedal pivot point about the axis on the bearing. Mathematically, the torque is the cross product of the lever-arm length vector, $\mathbf{L_c}$, and the force $\mathbf{F}_{\text{tan}}$ acting on the end of the lever-arm. Here, the lever-arm length is equal to the crank length L_c. Thus, the magnitude of the torque is given by

$$\|\boldsymbol{\tau}\| = \|\mathbf{L}_c \times \mathbf{F}_{\text{tan}}\| = L_c F_{\text{tan}}. \quad (7)$$

Figure 5 shows the torque patterns of one pedal for different pedalling styles, where a positive peak around 90° (downstroke) and a negative peak around 270° (upstroke) can be seen for all styles. The measurements were made in Korff, Romer, Mayhew, and Martin (2007) using a custom made force pedal with two triaxial piezoelectric force sensors, where 0° is highest position of the crank rotation.

The net torque τ_{net} is the sum of the individual torques τ_{left} and τ_{right} applied to the left and right pedals:

$$\tau_{\text{net}} = \tau_{\text{left}} + \tau_{\text{right}}. \quad (8)$$

Figure 6 shows an example of the net torque curve with some typical features to describe it.

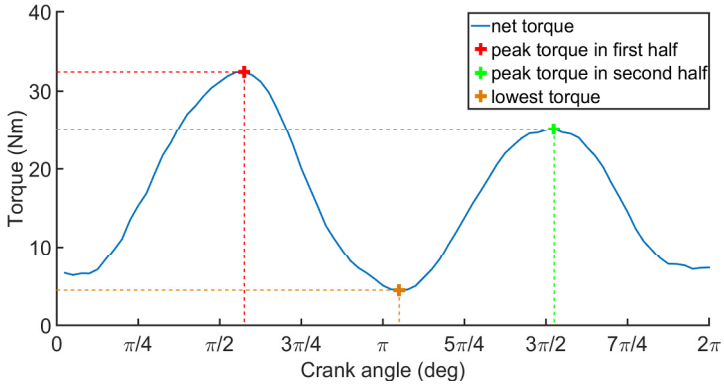

Figure 6 Mean of net torque τ_{net} for one pedal revolution with 60 rpm and 100 N ergometer brake force (i.e., 17.6 Nm).

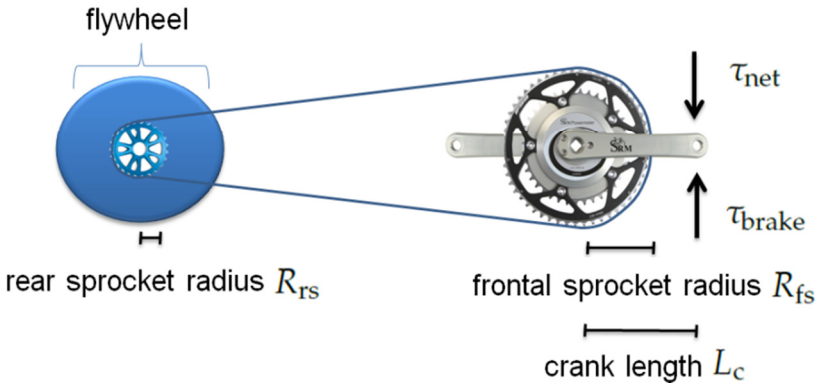

Figure 7 Basic model for the deduction of the torque equation.

For example, different peak values indicate an asymmetry due to emphasizing an unequal pushing action during the downstroke or due to a problem with pulling during the upstroke.

During the pedalling motion, two main torques act on the crank at the same time: the applied net torque τ_{net} and the brake torque τ_{brake}. τ_{net} is the sum of the individual pedal torques (Equation 8) and the brake pedal torque is the sum of all torques produced by the different forces against the cycling motion, e.g., the rolling and aerial resistive forces of a bicycle on the road, or the forces produced by an eddy-current brake in an ergometer in the lab.

Figure 7 shows a simple model of the torques acting during pedalling. In this model, the inertial mass of the cyclist and the bicycle is (partly) realised by the flywheel in the rear part of an ergometer. Assuming that the rear and frontal sprockets are connected with a chain which is not elastic and does not slip, and that the frictional forces between the chain and the sprockets are small, the physical relation between the torques τ_{net} and τ_{brake}, and the crank angular acceleration α_{crank}, is given by Equation 9. In this equation, $I_{flywheel}$ and I_{crank} represent the moments of inertia of the flywheel and the crank, R_{fs}/R_{rs} is the ratio of the radii of the chain wheel and the rear sprocket, i.e., the gear ratio, and L_c is the length of the crank,

$$\tau_{net} = \left(I_{crank} + \left(\frac{R_{fs}}{R_{rs}} \right)^2 I_{flywheel} \right) \cdot \alpha_{crank} + \tau_{brake} \,. \qquad (9)$$

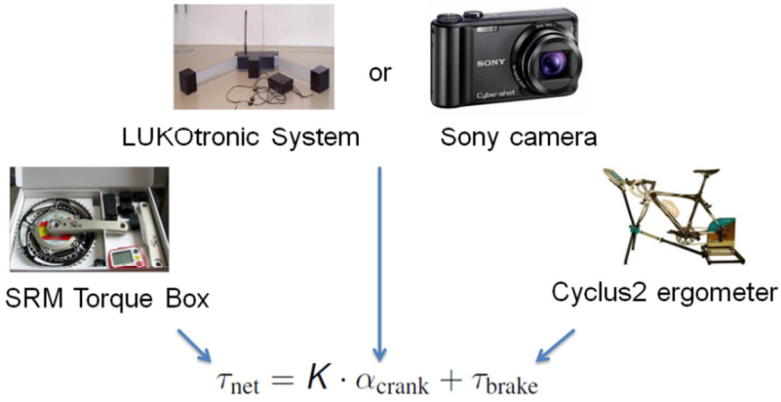

Figure 8 Equipment used for the experiment and their relation with the equation to validate. The angular crank acceleration was calculated from the data captured by the LUKOtronic System and the Sony camera.

Thus, the net torque is an (affine) linear function of the crank angular acceleration,

$$\tau_{\text{net}} = K \cdot \alpha_{\text{crank}} + \tau_{\text{brake}}, \quad (10)$$

with

$$K = \left(I_{\text{crank}} + \left(\frac{R_{\text{fs}}}{R_{\text{rs}}} \right)^2 I_{\text{flywheel}} \right). \quad (11)$$

Torque validation

Our goal was to determine to what extent net torques computed using Equation 9, based on numerically approximated crank acceleration from pedal motion measurements, are close to the directly measured (assumed to be true) net torques. For this purpose, we recorded the data simultaneously obtained from the motion capture system (i.e., MoCap data), the video camera recorder (i.e., video data), the bicycle ergometer, and the torque sensor, see Figure 8.

For the validation, we assumed that the angular crank acceleration α_{crank} is equal to the second derivative of angular position of the pivot of rotation of the pedal θ. To calculate the right-hand side of Equation 9, we used a crank length $L_c = 176$ mm, and moments of inertia

$I_{\text{flywheel}} = 0.6576\,\text{kg} \cdot \text{m}^2$ and $I_{\text{crank}} = 0.02\text{kg} \cdot \text{m}^2$. The gear ratio $R_{\text{fs}}/R_{\text{rs}}$ was calculated directly from the number of teeth on the gears in the gear train with $R_{\text{fs}} = 50$ and $R_{\text{rs}} = 13$. The inertia of the crank is composed of the inertia of the pedals, of the crank arm, of the chainrings, and of the SRM Power Meter. Each component can be approximated by a primitive geometric form rotating around the center of the crank axis (pedal - point mass, crank arm - solid cylinder, chainrings - rings, SRM - solid disc). We measured the weights and the sizes of each component and computed the individual moments of inertia. Their sum yields the total inertia of the crank $I_{\text{crank}} = 0.02\,\text{kg} \cdot \text{m}^2$, see more details in Dahmen and Saupe (2011). The moment of inertia of the flywheel was found empirically under the assumption that the friction force is an affine function of the velocity, which was verified through a fitting procedure. For this, we pedaled to accelerate the flywheel until it had a high speed. Then, we stopped pedalling and we counted the time until the flywheel did not move anymore.

The pipeline for calculating angular acceleration from positional data of the pedal is shown in Figure 9. The input is either the 3D MoCap data projected onto a two-dimensional plane using Principal Component Analysis (PCA), described in detail by Smith (2002), or the 2D

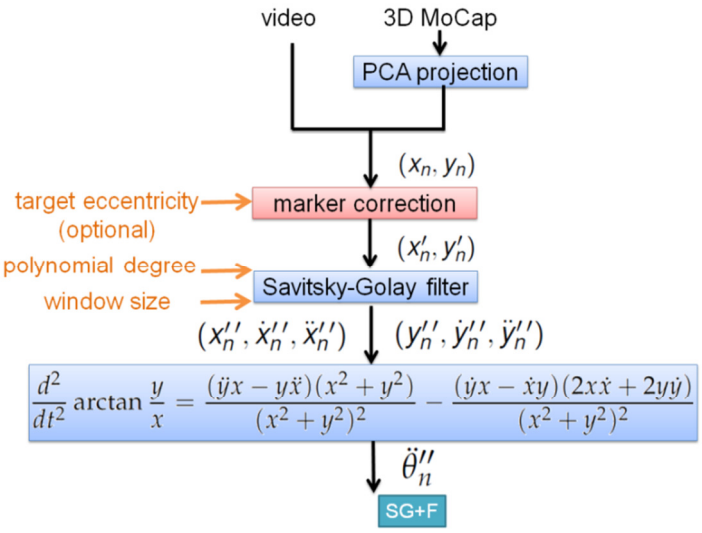

Figure 9 Pipeline for calculating angular crank acceleration from positional data. Parameters are given in orange. We assumed that the angular acceleration of the crank α_{crank} is equal to $\ddot{\theta}_n$.

positional video data. The correction of the marker position, explained in page 38, is a part of the preprocessing step (red module in Figure 9). We compared the results without this correction and with it based on two different methods, i.e., minimising the RMS distance between a fitted ellipse and the corrected data among all possible corrections and fitted ellipses, and with prescribed eccentricities. We tested the approach SG+F shown in Figure 9 consisted of the filtering and the calculation the zero, first and second derivatives of x and y coordinate sequences using the corresponding Savitzky-Golay filters for each case, and with this data then calculating the second derivative of θ using Equation 1.

Finally, the effects of correction of the marker position and filtering with different parameters were compared using the signal to noise ratio (SNR), where the true signal was assumed to be the SRM Torque Box data, and the noise was assumed to be the difference between the SRM Torque Box data and the right side of Equation 9.

Experimental setup

Data acquisition and processing

We recorded the pedalling motion using simultaneously a commercial camera (Sony Optical Steadyshot DSC–H55) and a motion capture system (LUKOtronic-Steinbichler Optotechnik GmbH, Neubeuern, Germany). The camera recorded videos with a sampling frequency of 29.97 Hz and a resolution of 1280×720 pixels. The video camera was placed at a distance of 270 cm from the bicycle.

The motion capture system consisted of a beam with three integrated infrared cameras. As a result of the fixed positions of the cameras within the beam, the system was pre-calibrated and did not require any separate calibration procedure. The motion capture system provided three-dimensional positional data of the infrared active markers. The sampling rate was 240 Hz. The positional accuracy provided by LUKOtronic for the distance used in our experiments was 1– 3 mm. Experimentally, the positional accuracy was 1.5 mm with a precision of 0.9 mm calculated from two markers fixed on the pedal during 180 crank rotations.

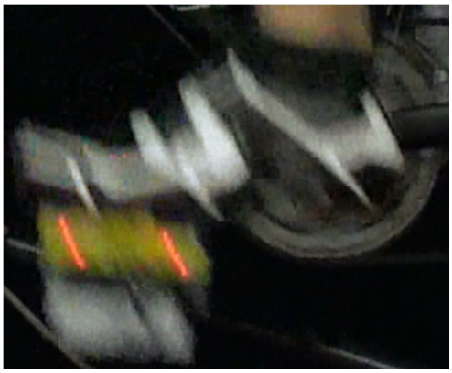

Figure 10 Example of LED trajectories as red streaks on yellow pedal in one video frame.

Using the motion capture system we recorded the position of two markers as shown in Figure 1. One marker was placed on the pivot point of the pedal rotation (i.e., a point representing the angular position of the crank during the motion of the pedal) and the other marker was placed on the right side next to the first marker. During the recording, we used three reference markers attached to the bicycle frame in order to define the coordinate system, which was re-calculated for each measurement. This has the advantage that oscillations and deflections of the bicycle frame due to the pedalling motion and bike sway are taken into account during the recording of the pedal motion. The pedal orientation for the motion data was calculated from the positional data of both markers with respect to the horizontal axis. We projected the three-dimensional coordinates of the marker position to a two-dimensional plane using the Principal Component Analysis (PCA). Then, we rotated the coordinate system using the information of additional measurements of the pedal in the lowest position.

Using the video camera we recorded two red LEDs placed on both sides of the pedal. See Figure 1. Each LED in a frame was captured as a streak due to blurring by the rapid movement of the pedal during the exposure time of the camera. See Figure 10 for an example. The LEDs were placed with enough space between them to avoid a possible streak overlapping. The coordinates of the heads of each streak were used in each frame as positional data of LEDs. The pivot point of the pedal was calculated as the average of both LED positions and the pedal orientation was calculated from the angle of the line between both LEDs with respect to the horizontal axis of the frame. For the detection of the streaks, each frame was converted from RGB format (i.e., red, green, and blue channels) to HSV format (i.e., hue H, saturation S, and value V). Then, a threshold on the value V was applied to find the blobs corresponding to the LED trajectories.

To control the pedal brake force, we used the Cyclus2 ergometer (RBM Elektronik-Automation GmbH, Leipzig, Germany). During the ergometer operation, the flywheel on the rear part is supplied with kinetic energy which maintains the angular momentum. The angular speed of the flywheel is decelerated by means of an eddy current brake. The eddy current brake guarantees a non-slipping transmission of the braking resistance. Operating the Cyclus2 in pedal force mode, a constant pedal brake force ($\pm 5\%$ error) is imposed.

Our SRM Torque Box (Schoberer Rad Messtechnik, Welldorf, Germany) gave an instantaneous torque signal with a sampling rate of 200 Hz. This torque corresponds to the net torque, as explained in Equation 8. Furthermore, when the crank has completed one pedal revolution (i.e., when the crank has crossed the sensor of the SRM Torque Box attached to the bicycle frame), this event was reported. SRM claims an accuracy of 2% for power and torque measurements.

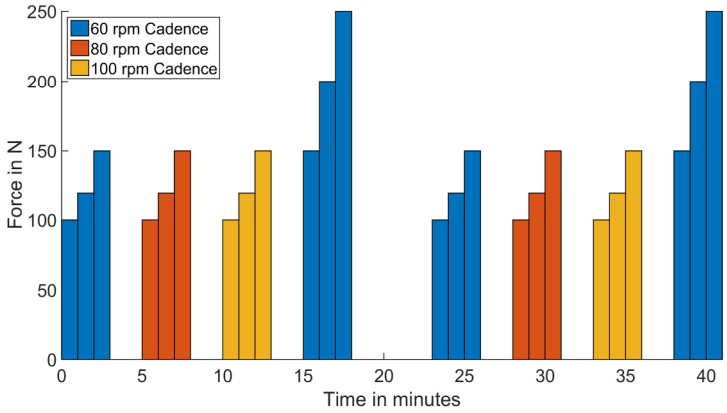

Figure 11 Experimental protocol. Eight test of three minutes each are performed with breaks of 2 resp. 5 minutes in between.

The laboratory conditions were optimized for recording the pedal motion: we darkened the room (i.e., we covered the window to avoid sunlight), used low infrared emitting light bulbs, and a special carpet to avoid infrared reflections from the ground.

Before the validation of the physical relation between the angular acceleration of the crank and the tangential force applied to the pedals, using Equation 9, we preprocessed the data obtained from all devices (see Figure 8). First, we applied linear interpolation when there was loss of data or outliers. Then, we resampled all data to 200 Hz. The data from all devices were registered using the SRM Torque Box data as reference. We used the information of the angular position of the crank when it crossed the sensor of SRM Torque Box attached to the bicycle frame in order to align the MoCap data and video with the SRM Torque Box data. The SRM Torque Box data and the Cyclus2 data were aligned using the time stamps provided by our system.

The correction of marker positions was performed using a quasi-Newton strategy minimizing either the difference between the prescribed eccentricity and the eccentricity of an ellipse fitted on the corrected positional data or the RMS distance between a fitted ellipse and the corrected data among all possible corrections and fitted ellipses. The ellipse fitting is performed by minimizing the squared sum of orthogonal distances from the points to the fitted ellipse described in Gander, Golub, and Strebel (1994).

Test design

Ten cyclists participated in this study (male, 31.45 ± 9.9 years). Each participant was asked to ride at a fixed cadence using his preferred technique and cycling shoes with cleats locked onto the pedal interface. A continuous feedback of the cadence was given on a projected video image, positioned in front of the cyclist. Before the measurements cyclists performed a warm up session of 5 minutes at a power output of 100 – 140 W.

Each subject rode the bike simulator performing eight tests of three minutes each. In each test the cadence was held constant and the brake force increased every minute. For the first three tests the cadences were 60 rpm, 80 rpm, and 100 rpm, and for each test the brake forces were 100 N, 120 N, and 150 N (i.e., brake torques of 17.6 Nm, 21.1 Nm and 26.4 Nm). For the fourth test, the cadence was again 60 rpm but with forces of 150 N, 200 N, and 250 N (i.e., brake torques of 26.4 Nm, 35.2 Nm and 44.0 Nm). This last test was done to check the effects of large forces on the SNR results which can vary due to crank deformation and brake force

fluctuation. All four tests were repeated once after a pause of 5 minutes. See Figure 11 for an illustration.

Results and discussion

Our goal was to determine to what extent net torques computed using Equation 9, based on numerically approximated crank acceleration from pedal motion measurements, are close to the directly measured (assumed to be true) net torques. For an example of the resulting torques, see Figure 12. We considered the following parameters of the Savitzky-Golay filter:

polynomial degrees $(2, 3)$ and window sizes $(10n + 1, n = 3, \dots, 22)$. We applied the Savitzky-Golay filter to the resampled data at 200 Hz. We also considered the results with and without the correction of marker positions, i.e., minimising the error between the fitted ellipse and corrected positional data (i.e., the minimum error eccentricity method) and with prescribed eccentricities $(e = 0.05i, i = 0, \dots, 6)$. See page 38 for a description of the methods for correction of marker position. Thus, we applied altogether for each test 360 different combinations of parameters and compared their SNR results.

Table 1 shows the average of the best SNR results for MoCap and video of all tests with and without marker correction among all parameter combinations. The SNR results with a marker correction and eccentricity 0 (i.e., a perfect circle) were the lowest for both MoCap and video data (see Table 1, column 4). This confirms that the crank and the bearings are elastic to a small degree and allow for some play.

Table 2 shows the average results for each test without marker correction and with marker correction based on M.E. for each combination of force and cadence. The marker correction based on M.E. improved the SNR results of the video data. These results were expected because in our video data recordings the position of the midpoint between LEDs cannot be precisely at the pivot point. The correction of the marker position based on M.E. did not improve the SNR results of the MoCap data. This indicates that the active infrared marker of the motion capture device was well placed on the pedal pivot point.

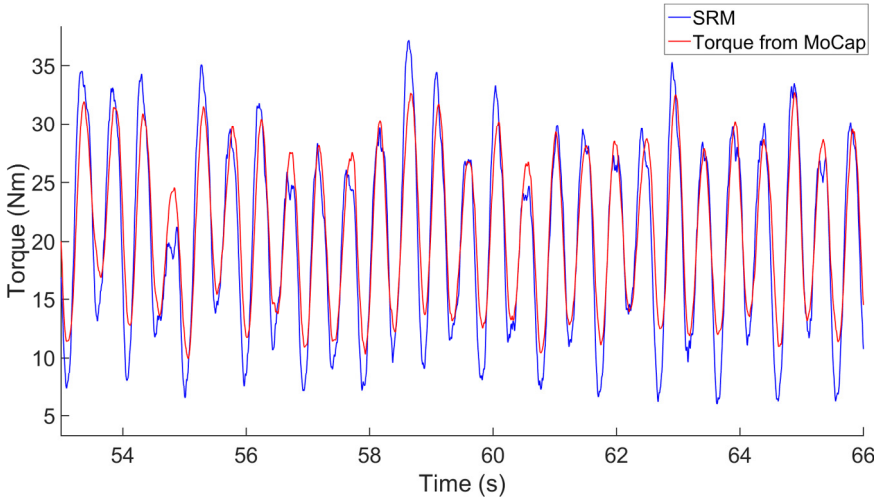

Figure 12 Result after alignment of SRM Torque Box data and MoCap data for the validation of the torque equation for the test with 60 rpm and 120 N (21.1 Nm) using the SG+F approach with window size 121, polynomial degree 2, and marker correction based on M.E.

Table 1 Average SNR for MoCap and video. Columns correspond to the type of input data, the SNR results without marker correction, the SNR results with M.E., and the results with different prescribed eccentricities for marker correction, respectively.

type	SNR	SNR e =M.E.	SNR $e = 0$	SNR $e = 0.15$	SNR $e = 0.2$	SNR $e = 0.25$	SNR $e = 0.3$
MoCap	14.82±1.86	14.67±1.75	9.74±1.97	13.28±2.04	14.74±1.94	15.12±1.96	14.80±2.11
video	10.81±2.11	12.30±2.47	9.61±2.18	11.60±1.84	13.42±1.75	14.02±1.78	14.18±2.11

Table 2 Average SNR of each test. The table shows the results for each combination of force and cadence. Columns correspond to brake force $\mathbf{F}_{\mathrm{brake}}$, cadence, the SNR results without marker correction and the results with marker correction based on M.E., respectively.

test		MoCap		video	
$\mathbf{F}_{\mathrm{brake}}$ N	cadence rpm	SNR $e = 0$	SNR e =M.E.	SNR $e = 0$	SNR e =M.E.
100	60	15.22±1.24	15.27±1.27	11.22±1.90	13.13±2.13
100	80	13.55±1.29	13.34±0.89	10.24±1.41	11.03±1.65
100	100	12.39±0.98	12.30±1.00	9.74±1.75	10.90±2.04
120	60	16.28±1.46	16.22±1.40	12.18±2.57	14.01±2.89
120	80	14.71±1.18	14.49±0.80	12.03±2.43	12.27±2.22
120	100	13.88±1.44	13.95±1.37	10.31±1.89	12.08±2.68
150	60	17.16±1.31	16.88±1.21	10.94±1.99	13.63±2.86
150	80	15.20±1.24	14.85±1.30	11.34±2.10	12.42±1.86
150	100	14.96±1.70	14.69±1.41	9.29±1.54	11.20±2.33
200	60	17.10±2.06	17.19±1.78	11.85±2.33	15.18±3.51
250	60	17.55±2.77	17.30±2.26	10.76±1.63	14.79±2.67

Table 3 Parameters for the best average SNR of the SG+F approach with marker correction based in two different methods. Columns correspond to type of data, brake force $\mathbf{F}_{\mathrm{brake}}$, cadence, polynomial degree and window size of the Savitsky-Golay filter employed for the method with prescribed eccentricities e, polynomial degree and window size of the Savitsky-Golay filter employed for the M.E. method, respectively.

			prescribed eccentricity			M.E.	
type	$\mathbf{F}_{\mathrm{brake}}$ N	cadence rpm	polynomial degree	window size	eccentricity	polynomial degree	window size
MoCap	100–150	60–100	2	121	0.25	2	91
MoCap	200	60	2	121	0.3	2	81
MoCap	250	60	3	191	0.2	3	191
video	100–150	60–100	2	121	0.25	2	81
video	200	60	3	171	0.25	3	201
video	250	60	3	181	0.2	3	201

The SNR results using the marker correction based on M.E. were lower than those obtained when fitting to ellipse with prescribed eccentricities. For example, the marker correction based on prescribed eccentricity $e = 0.25$ improved the SNR results for video ($+3.2$ dB) and slightly for MoCap ($+0.3$ dB), see Table 1. Figure 13 shows the effects on SNR results with different combinations of parameters of Savitsky-Golay filters and prescribed eccentricities for the tests with forces 100 N -150 N. The best results for both MoCap and video data were obtained with prescribed eccentricity $e = 0.25$, window size 121, and polynomial degree 2. For forces larger than 150 N another set of parameters provided the best results. These parameters are given in Table 3.

The deformation of trajectory of the point representing the angular position of the crank for the bicycle is difficult to obtain but possible, e.g., with torsional strain gauges at the crank. However, the strain gauges are the main component of several commercial torque meters that would allow direct toque measurements. In any case, the marker correction based on M.E. can improve the SNR results for the proposed video-based indirect torque measurements.

The differences between the torque based on the angular acceleration (obtained from the MoCap and video data) and the measured torque with SRM Torque Box might have arisen from the eddy current brake of the bicycle simulator. This brake is less than ideal, so that fluctuations in the pedal brake force could occur during our test. Furthermore, we assumed that the chain, the crank and the pedal are completely inelastic and non-slipping, and that the frictional forces between the chain and the gears is negligible compared with the pedal brake force produced by the eddy current brake of the Cyclus2 ergometer.

In addition, for the calculation of the crank acceleration it was assumed that the motion of the marker on the pedal pivot point lies in a two dimensional plane. This plane can be easily calculated from MoCap data projecting the 3D data onto 2D by using Principal Component Analysis (PCA) but with video data an additional reference to align the camera plane with the pedal motion plane is necessary to have better results. The positional data extracted from each video frame corresponded to the 2D projection of the crank motion plane to the camera plane. If these planes are not aligned, the projection of the circular trajectory of the crank motion to the camera plane results in an oval trajectory. Such misalignment of both planes may happen during the pedalling motion due to bike sway. This undesirable distortion could be minimized in each frame by a perspective correction based on some reference marker points on the bike frame.

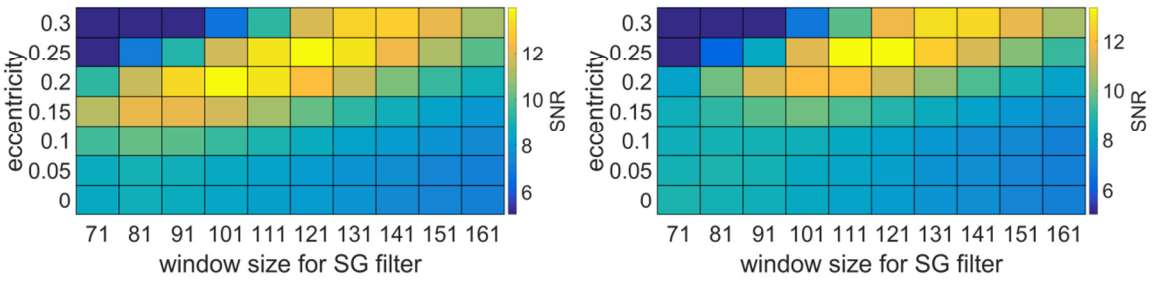

Figure 13 Mean SNR result of MoCap data (left) and video data (right) with correction of the marker position and different window sizes for the SG filter with degree 2 polynomials in the SG+F approach.

Conclusions

The physical relation between the angular acceleration of the crank and the tangential force applied to the pedals was validated with measured data of the net torque, brake force, video and MoCap data. These variables are related by an affine linear equation. The variation of the angular acceleration is proportional to the force variation when the pedal brake force is constant.

The proposed methods provided a valid calculation of the variation of the pedal acceleration (i.e., the torque variation). Our results show that optical motion tracking of the crank rotation can be used to estimate the tangential force variation applied to the pedal. The results obtained using a commercial video camera were close to the results achieved with a motion capture system, when a correction of the marker position was applied. Thus, an expensive optical device is not necessary to estimate the torque variation. We proposed values of the parameters for the relaxation and the Savitsky-Golay filter that can be used for pedal brake forces ranging between 100 and 250 N with cadences between 60 and 100 rpm for MoCap and video data. The training of a particular pedalling technique can be performed by providing athletes real-time performance feedback based on our proposed calculation of pedal torque variation. The only prerequisite is the availability of an ergometer delivering an adjustable constant pedal brake force, two LEDs on the pedal and a video camera.

For future research we intend to further improve our results with high speed camcorders (e.g., 59.94 fps) with a high image resolution. Furthermore, we plan to compensate the distortion due to bike sway performing a perspective correction with parameters calculated from the distortion of a reference attached to the bike frame.

Acknowledgments

This work was partially supported by the DFG Research Training Group GRK-1042 ”Explorative Analysis and Visualization of Large Information Spaces” and by the DFG project SA 449/12-1 “Powerbike: Model-based optimal control for cycling”[2] .

References

Bini, R. R., Diefenthaeler, F., & Mota, C. B. (2010). Fatigue effects on the coordinative pattern during cycling: Kinetics and kinematics evaluation. *Journal of Electromyography and Kinesiology*, *20*(1), 102–107.

Black, A. H. (1994). *The effect of steady rate exercise on the pattern of force production of the lower limbs in cycling*: University of British Columbia, Canada.

Böhm, H., Siebert, S., & Walsh, M. (2008). Effects of short-term training using SmartCranks on cycle work distribution and power output during cycling. *European Journal of Applied Physiology*, *103*(2), 225–232.

Cannon, D. T., Kolkhorst, F. W., & Cipriani, D. J. (2007). Effect of pedaling technique on muscle activity and cycling efficiency. *European Journal of Applied Physiology*, *99*(6), 659–664.

[2] https://www.informatik.uni-konstanz.de/saupe/forschung/laufende-projekte/powerbike/

Carpes, F. P., Rossato, M., Faria, I. E., & Bolli Mota, C. (2007). Bilateral pedaling asymmetry during a simulated 40-km cycling time-trial. *Journal of Sports Medicine and Physical Fitness*, *47*(1), 51–57.

Christensen, L., Johannsen, P., Sinkjær, T., Petersen, N., Pyndt, H. S., & Nielsen, J. B. (2000). Cerebral activation during bicycle movements in man. *Experimental Brain Research*, *135*(1), 66–72.

Dahmen, T., & Saupe, D. (2011). Calibration of a Power-Speed-Model for Road Cycling Using Real Power and Height Data. *International Journal of Computer Science in Sport*, *10*(2), 18–36.

Ettema, G., & Loraas, H. W. (2009). Efficiency in cycling: A review. *European Journal of Applied Physiology*, *106*(1), 1–14.

Faria, M. (2009). Recent advances in specific training for cycling. *International Sport Medicine Journal*, *10*(1), 16–32.

Höchtl, F., Böhm, H., & Senner, V. (2010). Prediction of energy efficient pedal forces in cycling using musculoskeletal simulation models. *Procedia Engineering*, *2*(2), 3211–3215.

Gander, W., Golub, G. H., & Strebel, R. (1994). Least-squares fitting of circles and ellipses. *BIT Numerical Mathematics*, *34*(4), 558–578.

Hamming, R. W. (1989). *Digital Filters*. *Dover Civil and Mechanical Engineering Series*: Dover Publications.

Hug, F., Turpin, N. A., Guével, A., & Dorel, S. (2010). Is interindividual variability of EMG patterns in trained cyclists related to different muscle synergies? *Journal of Applied Physiology*, *108*(6), 1727–1736.

Hull, M. L., Kautz, S., & Beard, A. (1991). An angular velocity profile in cycling derived from mechanical energy analysis. *Journal of Biomechanics*, *24*(7), 577–586.

Jirsa, V. K., Fink, P., Foo, P., & Kelso, J. A. (2000). Parametric stabilization of biological coordination: A theoretical model. *Journal of Biological Physics*, *26*(2), 85–112.

Kautz, S. A., & Hull, M. L. (1993). A theoretical basis for interpreting the force applied to the pedal in cycling. *Journal of Biomechanics*, *26*(2), 155–165.

Korff, T., Romer, L. M., Mayhew, I., & Martin, J. C. (2007). Effect of pedaling technique on mechanical effectiveness and efficiency in cyclists. *Medicine and Science in Sports and Exercise*, *39*(6), 991–995.

Mornieux, G., Zameziati, K., Mutter, E., Bonnefoy, R., & Belli, A. (2006). A cycle ergometer mounted on a standard force platform for three-dimensional pedal forces measurement during cycling. *Journal of Biomechanics*, *39*(7), 1296–1303.

Orfanidis, S. J. (2010). *Introduction to Signal Processing*. *Prentice Hall international editions*: Prentice Hall.

Ovaska, S. J., & Valiviita, S. (1998). Angular acceleration measurement: A review. *IEEE Transactions on Instrumentation and Measurement*, *47*(5), 1211–1217.

Press, W. H., Teukolsky, S. A., Vetterling, W. T., & Flannery, B. P. (2007). *Numerical Recipes 3rd Edition: The Art of Scientific Computing* (3rd ed.): Cambridge University Press.

Rossato, M., Bini, R. R., Carpes, F. P., Diefenthaeler, F., & Moro, A. (2008). Cadence and workload effects on pedaling technique of well-trained cyclists. *International Journal of Sports Medicine*, *29*(9), 746–752.

Sanderson, D. J. (1990). The influence of cadence and power output on asymmetry of force application during steady-rate cycling. *Journal of Human Movement Studies*, *19*, 1–9.

Savitzky, A., & Golay, M. J. E. (1964). Smoothing and differentiation of data by simplified least squares procedures. *Analytical Chemistry*, *36*(8), 1627–1639. doi:10.1021/ac60214a047

Schafer, R. W. (2011). What is a Savitzky-Golay filter? *Signal Processing Magazine, IEEE*, *28*(4), 111–117.

Smak, W., Neptune, R. R., & Hull, M. L. (1999). The influence of pedaling rate on bilateral asymmetry in cycling. *Journal of Biomechanics*, *32*(9), 899–906.

Stapelfeldt, B., Mornieux, G., & Gollhofer, A. (2006). Wirkung von Feedback-Training im Radsport auf physiologische und biomechanische Parameter. *BISp-Jahrbuch Forschungsförderung*, *7*, 175–179.

Stapelfeldt, B., Mornieux, G., Oberheim, R., Belli, A., & Gollhofer, A. (2007). Development and evaluation of a new bicycle instrument for measurements of pedal forces and power output in cycling. *International Journal of Sports Medicine*, *28*(4), 326–332.

Theurel, J., Crepin, M., Foissac, M., & Temprado, J. J. (2011). Effects of different pedalling techniques on muscle fatigue and mechanical efficiency during prolonged cycling. *Scandinavian Journal of Medicine & Science in Sports*, *22*(6), 714–721.